1521-0111/102/6/240–247$35.00
MOLECULAR PHARMACOLOGY

dx.doi.org/10.1124/molpharm.122.000525
Mol Pharmacol 102:240–247, December 2022



# Structural Basis for the Allosteric Inhibition of Hypoxia-Inducible Factor 2 by Belzutifan

Xintong Ren, Xiaotong Diao, Jingjing Zhuang, and Dalei Wu

*Helmholtz International Laboratory, State Key Laboratory of Microbial Technology, Shandong University, Qingdao, China (X.R., X.D., J.Z., D.W.) and Marine College, Shandong University, Weihai, China (J.Z.).*

Received March 2, 2022; accepted September 5, 2022

## ABSTRACT

Hypoxia-inducible factor (HIF)-2α and its obligate heterodimerization partner aryl hydrocarbon receptor nuclear translocator (ARNT), are both members of the basic helix-loop-helix-PER-ARNT-SIM transcription factor family. Previous studies have identified HIF-2α as a key oncogenic driver in clear cell renal cell carcinoma (ccRCC), rendering it a promising drug target for this type of kidney cancer. Belzutifan is the first HIF-2α inhibitor approved for treating ccRCC and other cancers associated with the von Hippel-Lindau disease. However, the detailed inhibitory mechanism of belzutifan at molecular level is still unclear. Here we obtained the crystal structure of HIF-2α–ARNT heterodimer in complex with belzutifan at 2.75 Å resolution. The complex structure shows that belzutifan binds into the PAS-B pocket of HIF-2α, and it destabilizes the dimerization of HIF-2α and ARNT through allosteric effects mainly mediated by the key residue M252 of HIF-2α near the dimer interface. We further explored the inhibitory effects of belzutifan using biochemical and functional assays. The time-resolved fluorescence energy transfer–based binding assay showed that belzutifan disrupts the dimerization of HIF-2α and ARNT with a $K_i$ value of 23 nM. The luciferase reporter assay indicated that belzutifan can efficiently inhibit the transcriptional activity of HIF-2α with an $IC_{50}$ value of 17 nM. Besides, the real-time polymerase chain reaction assay illustrated that belzutifan can reduce the expression of HIF-2α downstream genes in 786-O kidney cancer cells in a dose-dependent manner. Our work reveals the molecular mechanism by which belzutifan allosterically inhibits HIF-2α and provides valuable information for the subsequent drug development targeting HIF-2α.

## SIGNIFICANCE STATEMENT

The basic helix-loop-helix-PER-ARNT-SIM (bHLH-PAS) family of transcription factors are an emerging group of small-molecule drug targets. Belzutifan, originally developed by Peloton Therapeutics, is the first Food and Drug Administration–approved drug directly binding to a bHLH-PAS protein, the hypoxia-inducible factor (HIF)-2α. Based on the protein-drug complex structure, biochemical binding assays, and functional profiling of downstream gene expression, this study reveals the regulatory mechanism of how belzutifan allosterically destabilizes HIF-2α's heterodimerization with its obligate partner protein, thus reducing their transcriptional activity that links to tumor progression.

## Introduction

Hypoxia-inducible factors (HIFs) are a group of transcription factors that belong to the basic helix-loop-helix-PER-ARNT-SIM family, each possessing a basic helix-loop-helix domain and two PAS (PAS-A and PAS-B) domains near the protein N-terminus (Wu and Rastinejad, 2017). HIFs can regulate sensing and adaptation of cells to oxygen availability (Wang et al., 1995). Transcriptionally active HIF complexes are heterodimers composed of an oxygen-sensitive α subunit (HIF-α) and a constitutively expressed β subunit, which is usually called the aryl hydrocarbon receptor nuclear translocator (ARNT). In vertebrates, three HIF-α isoforms (HIF-1α, HIF-2α, and HIF-3α) encoded by separate genes have been identified (Wang et al., 1995; Tian et al., 1997;Gu et al., 1998). The mechanism of how HIF-α proteins are responsive to cellular oxygen level through the oxygen-dependent hydroxylation and following proteasomal degradation, which is mediated by the von Hippel Lindau (VHL) tumor suppressor via ubiquitination (Huang et al., 1998), has been investigated thoroughly and recognized by the 2019 Nobel Prize in Physiology or Medicine (Zhang, Yan et al., 2019).

HIFs regulate transcription of genes related to cell proliferation (Gordan et al., 2007), angiogenesis (Yoshimura et al., 2004; Rankin et al., 2007), cell migration (Esteban et al., 2006), and resistance to anticancer therapies (Zhao et al., 2015); thus, they may contribute to tumor survival and serve as potential drug targets. Expression of HIF-2α has been found to correlate with the progression and poor prognosis of several tumors, including head and neck squamous cell carcinoma (Winter et al., 2006), as well as lung (small and non-small cells) (Liu et al., 2006; Luan et al., 2013), colorectal (Yoshimura et al., 2004), liver

This work was supported by the Shandong Provincial Natural Science Foundation, China [Grant ZR2021JQ30], the National Natural Science Foundation of China [Grant 22177063], Interdisciplinary Innovative Research Group Program of Shandong University [Grant 2020QNQT009], the National Key R&D Program of China [Grant 2018YFE0113000], and the Taishan Scholars Program of Shandong [Grant tsqn201909004] to D.W.

No author has an actual or perceived conflict of interest with the contents of this article.

dx.doi.org/10.1124/molpharm.122.000525.

**ABBREVIATIONS:** ARNT, aryl hydrocarbon receptor nuclear translocator; ccRCC, clear cell renal cell carcinoma; HIF, hypoxia-inducible factor; HRE, hypoxia response element; ITC, isothermal titration calorimetry; PCR, polymerase chain reaction; TR-FRET, time-resolved fluorescence energy transfer; VHL, von Hippel-Lindau; WT, wild-type.

(Bangoura et al., 2007), and kidney (Xia et al., 2001) cancers. Due to the gene deficiency of *VHL*, vast majority (about 90%) of patients with clear cell renal cell carcinoma (ccRCC) encounter a stable presence of HIF-$\alpha$ that promotes the survival of cancer cells (Sato et al., 2013). Moreover, it has been found that the HIF-1$\alpha$ isoform is usually missing or mutated in ccRCC, while the overexpressed HIF-2$\alpha$ functions as a critical driver (Shen and Kaelin, 2013). Therefore, selectively inhibiting the activity of HIF-2$\alpha$ can potentially block the progression of ccRCC.

The identification of HIF-2$\alpha$ inhibitors is a classic structure-based drug discovery process. Scheuermann et al. (2009) reported the crystal structure of human HIF-2$\alpha$–ARNT heterodimer containing only the PAS-B domains of both proteins. This crystal structure revealed a hydrophobic cavity of 290 $Å^3$ within HIF-2$\alpha$ and enabled a screening campaign for HIF-2$\alpha$ inhibitors targeting the PAS-B cavity (Key et al., 2009). In the following years, they reported more artificial HIF-2$\alpha$ ligands that antagonized the heterodimerization of HIF-2$\alpha$–ARNT and displayed improved cellular activities (Rogers et al., 2013; Scheuermann et al., 2013; Scheuermann et al., 2015). One of those ligands, N-(3-chloro-5-fluorophenyl)-4-nitro-2,1,3-benzoxadiazol-5-amine (also called 0X3), was used as a starting point for the further design of HIF-2$\alpha$ inhibitors. This work was led by scientists at Peloton Therapeutics who in 2018 disclosed the discovery of PT2385 (Fig. 1A), the first HIF-2$\alpha$ small-molecule inhibitor entering clinical trials for the treatment of ccRCC (Wehn et al., 2018). However, in the trial, a large proportion of patients were underexposed with little clinical benefit due to the unexpected strong metabolism of PT2385 to its glucuronide metabolite. In 2019, they reported belzutifan (also called PT2977 or MK-6482) (Fig. 1B), a new HIF-2$\alpha$ inhibitor with improved pharmacokinetic properties by changing the geminal difluoro group of PT2385 to a vicinal difluoro group (Xu et al., 2019). In the same year, Merck Sharp & Dohme Corp. acquired Peloton Therapeutics. In August 2021, the US Food and Drug Administration approved belzutifan for adult patients with VHL disease who require a therapy for associated renal cell carcinoma, central nervous system hemangioblastomas, or pancreatic neuroendocrine tumors not requiring immediate surgery.

We previously solved the crystal structure of multidomain HIF-2$\alpha$–ARNT heterodimer in complex with PT2385 (Wu et al., 2019). However, the structure of HIF-2$\alpha$–ARNT bound with belzutifan is still not available, limiting further understanding of its detailed mechanism of action. Here, we report the crystal structure of HIF-2$\alpha$–ARNT-belzutifan complex. Our results indicate that belzutifan bound into the PAS-B domain pocket of HIF-2$\alpha$ and disrupted the dimerization of HIF-2$\alpha$ and ARNT through allosteric effects initiated largely by the side chain conformational change of HIF-2$\alpha$ residue M252. We further determined the inhibitory effects of belzutifan against HIF-2$\alpha$ at both molecular and cellular levels. This work reveals the mechanism of how belzutifan inhibits the transcriptional activity of HIF-2$\alpha$ and provides valuable information for the future design of HIF-2$\alpha$–targeting drugs.

## Materials and Methods

**Compounds and Other Materials.** Belzutifan and PT2385 were purchased from MedChemExpress (MCE). Tacsimate, PEG3350, and other crystallization reagents were from Sigma-Aldrich. $\beta$-D-

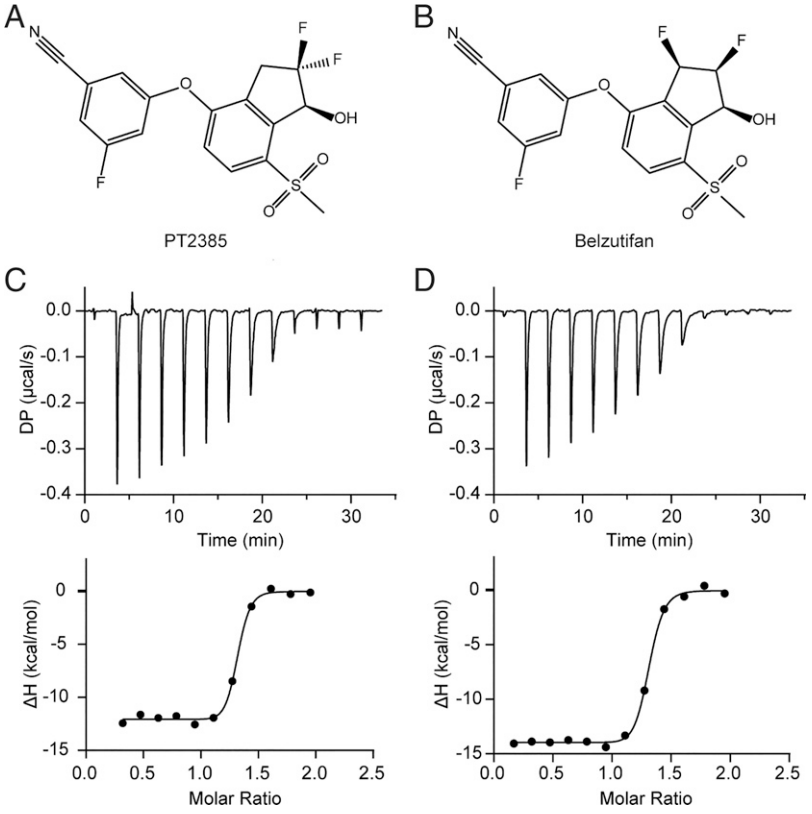


**Fig. 1.** Comparison of the HIF-2$\alpha$–binding affinities between PT2385 and belzutifan. (A and B) Chemical structures of PT2385 (A) and belzutifan (B). (C and D) Binding of PT2385 (C) and belzutifan (D) to the HIF-2$\alpha$ PAS-B domain as measured by ITC. The calculated $K_D$ value of PT2385 was 10 ± 4.9 nM, while the $K_D$ value of belzutifan was 16 ± 4.7 nM. This experiment was independently repeated twice.

thiogalactopyranoside and dithiothreitol were from Dingguo Biotechnology. All other reagents and solvents are also commercially available and at analytical grade.

**Plasmid Construction, Protein Expression, and Purification.** Recombinant expression plasmids containing the N-terminal basic helix-loop-helix-PER-ARNT-SIM regions of mouse HIF-2$\alpha$ and ARNT proteins, including wild-type (WT) pSJ2-HIF-2$\alpha$ (3-361), pSJ2-HIF-2$\alpha$ (3-361) M252A mutant, and pMKH-ARNT (82-464); as well as the pSJ2-HIF-2$\alpha$ (241-361) for the single PAS-B domain of HIF-2$\alpha$ used in the binding assay; pMKH-ARNT-GFP (82-464) for GFP-tagged ARNT used in the time-resolved fluorescence energy transfer (TR-FRET) assay; and pCMV-Tag4-HIF-2$\alpha$ full-length plasmids (WT or M252A mutant) used in the real-time polymerase chain reaction (PCR) assay, were all constructed as described previously (Wu et al., 2019).

Proteins were expressed and purified in a similar manner as previously described (Wu et al., 2019). Briefly, to obtain HIF-2$\alpha$–ARNT complex proteins, the pSJ2-HIF-2$\alpha$ plasmid and pMKH-ARNT plasmid were co-transformed into *E. coil* BL21 CodonPlus. Following 0.1 mM $\beta$-D-thiogalactopyranoside induction overnight at 16°C, cells were lysed by sonication. Supernatants were purified by nickel-nitrilotriacetic acid affinity resin (GE Healthcare) and SP affinity resin (GE Healthcare), followed by size exclusion chromatography using a 16/60 Superdex 200 pg gel-filtration column (GE Healthcare). The heterodimeric proteins of HIF-2$\alpha$ and ARNT-GFP were prepared similarly, except that the pMKH-ARNT-GFP plasmid was used in the place of pMKH-ARNT. Purification of the single PAS-B domain of HIF-2$\alpha$ was conducted similarly, except for the skipped step of cation exchange chromatography.

**Isothermal Titration Calorimetry Binding Assay.** Isothermal titration calorimetry (ITC) experiments were performed using a PEAQ-ITC (Malvern) instrument at 25°C. PT2385, belzutifan, and the HIF-2$\alpha$ PAS-B proteins were respectively dissolved in a buffer containing 20 mM Tris-HCl (pH 8.0), 400 mM NaCl and 2% DMSO. Then, 40 $\mu$L of 100 $\mu$M PT2385 or belzutifan was continuously added to titrate the 10 $\mu$M HIF-2$\alpha$ protein. The first injection was 0.4 $\mu$L, and the 12 subsequent injections were 3.0 $\mu$L each. The time interval between two drops was 150 seconds. The site-binding model was determined by using MicroCal PEAQ-ITC Analysis Software, and binding isotherm data were fitted by the GraphPad Prism software.

**Crystallization, Data Collection, and Structure Determination.** HIF-2$\alpha$–ARNT protein complexes were crystallized by mixing equal volume of protein and the reservoir containing Tacsimate (pH 7.0) and PEG3350 using the sitting-drop vapor diffusion method at 16°C. After a series of trials on soaking conditions, crystals of HIF-2$\alpha$–ARNT-belzutifan complex were finally obtained by adding compounds (100 $\mu$M) to the drops containing *apo* protein crystals and soaking for 8 hours before crystal harvest. Diffraction data were collected at Shanghai Synchrotron Radiation Facility 19U beamline (Zhang, Tang et al., 2019) and processed using the XDS program (Kabsch, 2010).

The structure of HIF-2$\alpha$–ARNT-belzutifan complex was solved by molecular replacement with the program Phaser (McCoy et al., 2007), using the *apo* HIF-2$\alpha$–ARNT structure (PDB code 4ZP4) as the search model. Further manual model building was facilitated by using Coot (Emsley et al., 2010), combined with the structure refinement using Phenix (Adams et al., 2010). The final model was validated by MolProbity (Chen et al., 2010). A summary of diffraction data and final statistics can be found in Table 1. Molecular graphics for figures were prepared with PyMOL (PyMOL Molecular Graphics System, version 2.3.0; Schrödinger, LLC).

**TR-FRET-Based Binding Assay.** Similar to our previous work, purified protein complexes of GFP-tagged ARNT and HIF-2$\alpha$ were dispensed into 384-well plates, with serial dilutions of belzutifan, in the assay buffer containing 20 mM HEPES (pH 7.5), 400 mM NaCl, 10 mM dithiothreitol, and 0.5% Tween-20. After addition of the Terbium-labeled anti-His antibody (Cisbio, 61HI2TLF) into each well, the plate was kept in dark for 3 hours. The protein interactions were monitored via the energy transfer signal with a Spark multimode microplate reader (Tecan). The TR-FRET value was determined as a ratio of the signal measured at 520 nm (GFP) to the signal measured at 340 nm (terbium). The apparent $K_i$ value of belzutifan toward HIF-2$\alpha$–ARNT complex was calculated by plotting the ratios (520 nm/340 nm) against the compound concentrations (Wu et al., 2019).

**Luciferase Reporter Assay.** 786-O cells with a stable-transfected hypoxia response element (HRE)-luc reporter were kindly provided by Prof. Fraydoon Rastinejad at University of Oxford. The cells were seeded in RPMI1640 medium with 10% FBS in 48-well plates and treated with belzutifan at different concentrations (final DMSO concentration kept at 0.1%) when the cell density was close to 60%. After 24 hours of incubation, cells were lysed and analyzed using Steady-Glo Luciferase Assay System (Promega, E2510).

**Real-Time PCR Assay.** 786-O cells (Dingguo Biotechnology, CS0254) were cultured in RPMI1640 medium with 10% FBS in 12-well plates at 37°C in 5% $CO_2$. When cells grew to 60% density, different concentrations of belzutifan were added with a final DMSO concentration kept at 0.1%. After 24 hours of treatment, cells were collected and RNA was extracted using RNAiso Plus (Takara), followed by cDNA synthesis using PrimeScript RT reagent Kit with gDNA Erase (Takara).

Hep3B cells (Dingguo Biotechnology, CS0172) were cultured in DMEM medium with 10% FBS in 12-well plates at 37°C in 5% $CO_2$. When cells grew to 60% density, they were transfected with pCMV-Tag4-HIF-2$\alpha$ plasmids (WT or M252A mutant). Medium was refreshed after 6 hours of transfection, and cells were treated with 10 $\mu$M belzutifan in 0.1% DMSO for 36 hours in 5% $CO_2$ before RNA isolation.

HEK293 cells (Dingguo Biotechnology, CS0001) were cultured in DMEM medium with 10% FBS in 12-well plates at 37°C in 5% $CO_2$. When cells grew to 60% density, different concentrations of belzutifan were added with the final DMSO concentration kept at 0.1%. Cells were cultured for 24 hours in 1% $O_2$ before RNA isolation.

Real-time PCR was conducted on a step-two system using Hieff qPCR SYBR Green Master Mix (Yeasen). The expression levels of target genes were normalized to the expression of $\beta$-actin (ACTB). PCR primers were synthesized by Personalbio Technology as follows: ACTB (F: GCACAGAGCCTCGCCTT, R: GTTGTCGACGACGAGCG), CyclinD1 (F: TGGAGCCCGTGAAAAAGAGC, R: TCTCCTTCATCTTAGAGGCCAC), NDRG1 (F: CTCCTGCAAGAGTTTGATGTCC, R: TCATGCCGATGTCATGGTAGG), EPO (F: GGAGGCCGAGAATATCACGAC, R: CCCTGCCAGACTTCTACGG), VEGFA (F: TACCTCCACCATGCCAAGTG, R: ATGATTCTGCCCTCCTCCTTC), and GLUT1 (F: TCTGGCATCAACGCTGTCTTC, R: CGATACCGGAGCCAATGGT).

TABLE 1
Data collection and refinement statistics

| | HIF-2$\alpha$–ARNT-belzutifan |
|---|---|
| PDB ID | 7W80 |
| **Data collection** | |
| Space group | P 21 |
| Cell constants | |
| a, b, c (Å) | 49.19, 98.19, 77.74 |
| $\alpha$, $\beta$, $\gamma$ (°) | 90, 107.16, 90 |
| Resolution (Å) | 50.00 - 2.75 |
| Rmerge | 0.06 |
| I/$\sigma$I | 1.98 (at 2.75 angstrom) |
| Completeness (%) | 99.7 |
| Redundancy | 6.8 |
| **Refinement** | |
| Resolution | 46.38 - 2.75 |
| Reflections, n | 18322 |
| R-work, R-free | 0.216, 0.274 |
| Atoms, n | |
| Protein | 4406 |
| Ligand/ion | 26 |
| B-factors | |
| Protein | 87.71 |
| Ligand/ion | 59.51 |
| R.m.s. deviations | |
| Bond lengths (Å) | 0.01 |
| Bond angles (°) | 1.24 |

**Data Analysis.** Data are expressed as the mean ± S.D. $K_i$ and $IC_{50}$ values were derived from a four-parameter logistic equation.

## Results

**Binding Affinity of Belzutifan to HIF-2α Protein.** As mentioned earlier, belzutifan is the second-generation HIF-2α inhibitor with increased potency and improved pharmacokinetic profile achieved by reduction of phase 2 metabolism (Xu et al., 2019). To test whether belzutifan maintains a similar binding affinity to its target HIF-2α in comparison with the first-generation inhibitor PT2385, we measured the binding affinities of belzutifan and PT2385 to HIF-2α using an ITC assay with purified proteins of the single PAS-B domain. The calculated $K_D$ value of PT2385 was 10 ± 4.9 nM (Fig. 1C), while the $K_D$ value of belzutifan was 16 ± 4.7 nM (Fig. 1D), suggesting no big difference in binding affinities between the two inhibitors. Our results indicate that the structural modification of changing the geminal difluoro group in PT2385 to a vicinal difluoro group in belzutifan had no dramatic influence on their binding affinity to HIF-2α protein. Therefore, the better potency of belzutifan in the clinical trial might largely come from its in vivo stability and resistance to drug metabolism.

**The Crystal Structure of HIF-2α–ARNT–Belzutifan Complex.** To further explore the inhibitory mechanism of belzutifan at the molecular level, we sought to first reveal the structural information about how belzutifan binds into HIF-2α. For crystallization, we co-expressed and purified mouse HIF-2α and ARNT proteins that both contain their N-terminal basic helix-loop-helix and tandem PAS domains (Fig. 2A), in a heterodimeric form. It is noteworthy that the originally reported crystal structure of the HIF-2α–ARNT protein complex only contains two PAS-B domains, which formed a stable dimer with the help from an artificial salt bridge generated by point mutations (Scheuermann et al., 2009). However, since this artificial salt bridge across the dimer interface introduced additional interactions to further enhance the dimerization, it is hard to interpret how inhibitors binding into the PAS-B domain of HIF-2α exert their dimer-disrupting effects. In contrast, our multidomain dimeric protein complex was stabilized by native interdomain interactions, which can likely represent their physiologic status in cells and more importantly help delineate the potential allosteric effects of HIF-2α inhibitors (Wu et al., 2015).

Directly through co-crystallization, we were unable to obtain belzutifan-bound HIF-2α–ARNT protein crystals in a good quality, probably due to the strong destabilizing effects of belzutifan (Xu et al., 2019). Therefore, instead, we soaked belzutifan into the *apo* HIF-2α–ARNT protein crystals by a series of trials on the proper drug concentrations as well as duration time and successfully obtained diffractable crystals. We then solved the structure of HIF-2α–ARNT dimer in complex with belzutifan at 2.75 Å resolution. As shown in Fig. 2B, belzutifan binds into the PAS-B domain pocket of HIF-2α, evidenced by the clear electron density maps within the pocket (Fig. 2, C and D). Belzutifan shares a hydrogen bond with the side chain of residue H293, thus stabilizing the binding pose of this drug (Fig. 2E). In addition, belzutifan forms a π–π interaction with F254 and numerous hydrophobic interactions with neighboring residues (Fig. 2E).

The binding mode of belzutifan is roughly very similar to that of PT2385, which also binds into the PAS-B pocket of HIF-2α and forms a hydrogen bond with H293 (Fig. 2F) (Wu et al., 2019). This mode similarity between belzutifan and PT2385 (Fig. 2, G and H), correlates well with their comparable binding affinities to HIF-2α (Fig. 1, C and D).

**Conformational Changes of HIF-2α–ARNT on Belzutifan Binding.** To reveal the detailed mechanism of how belzutifan disrupts the dimerization of HIF-2α–ARNT, we first checked the protein conformational changes upon belzutifan binding. When superimposing the belzutifan-bound HIF-2α–ARNT structure onto the unbound "*apo*" structure (PDB code 4ZP4), we found a clear conformational change near the dimerization interface between HIF-2α and ARNT PAS-B domains (Fig. 3, A and B). Binding of belzutifan forced the side chain of HIF-2α M252 residue to flip out of the pocket, potentially destroying the stability of the dimerization interface between the HIF-2α PAS-B domain and the ARNT PAS-B domain. As a result, the loop regions on both sides of the interface also exhibited shifts in their conformation and position (Fig. 3B).

Previously we adopted a hydrogen-deuterium exchange mass spectrometry assay to reveal the overall conformational changes of multidomain HIF-2α–ARNT protein complex caused by HIF-2α ligands (Wu et al., 2019). In addition to the dimer interface between two PAS-B domains, binding of PT2385 (and another inhibitor named T1001) allosterically induced destabilizing effects at other domain–domain junctions along the interface, as evidenced by the increased hydrogen–deuterium exchange rates (Wu et al., 2019). Here since belzutifan binds into HIF-2α in a nearly identical fashion to PT2385 (Fig. 2H), it would probably share a similar inhibitory mechanism of reducing the HIF-2 transcriptional activity by allosterically disrupting heterodimerization.

In addition, we also highlighted the key role of HIF-2α M252 residue in mediating the allosteric mechanism in our previous study (Wu et al., 2019). The M252A mutation could abolish inhibitory effects of PT2385 on both HIF-2α–ARNT heterodimerization and the transcriptional activity of downstream genes. Moreover, by comparing various inhibitors, we noticed that the movement extent of M252's side chain from inside of HIF-2α PAS-B pocket toward the dimer interface positively correlates with the potency of different inhibitors (Wu et al., 2019). As shown in Fig. 3C, in the crystal structure of HIF-2α–ARNT-belzutifan complex, M252 was pushed out of the pocket by belzutifan to a similar position as that by PT2385, suggesting these two compounds may possess close inhibitory activities in biochemical and cellular systems.

**Determination of the Inhibitory Effects on HIF-2α by Belzutifan.** To further confirm the allosteric and inhibitory effects of belzutifan on HIF-2α, we conducted both biochemical and functional assays. First, we adopted a TR-FRET–based direct-binding assay, in which interactions between HIF-2α and ARNT could be detected by the energy transfer between donor and acceptor molecules respectively coupled to the two subunits. As shown in Fig. 4, A and B, belzutifan disrupted the dimerization of WT HIF-2α and ARNT with a $K_i$ value of approximately 23 nM, while its $K_i$ value for HIF-2α M252A mutant was dramatically increased to about 3.5 μM, supporting the idea that M252 plays a key role in mediating the allosteric regulation of belzutifan on dimerization. It has to be pointed out that the maximum heterodimer disruption ratio was only around 50% in this assay, indicating the disassociation of dimerized HIF-2α–ARNT proteins was not complete even at a very high concentration of belzutifan. These results suggest that in the in vitro systems using co-expressed recombinant

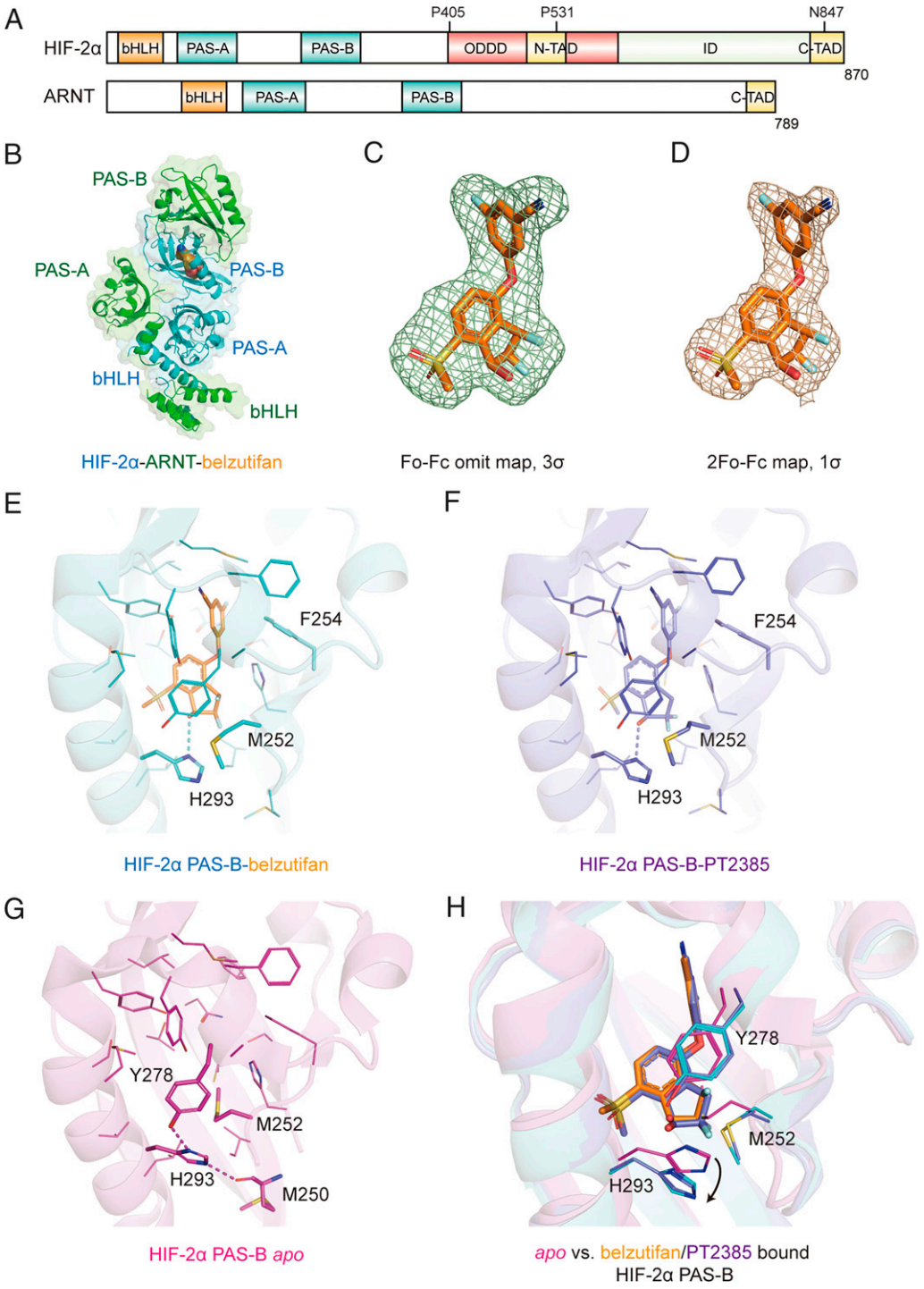


**Fig. 2.** Crystal structure of the HIF-2α–ARNT-belzutifan complex. (A) Schematic representation showing the domain arrangements of HIF-2α and ARNT. (B) Binding position for belzutifan (brown) within the entire HIF-2α–ARNT crystal structure. (C) $F_O$–$F_C$ omit map of belzutifan contoured at 3σ. (D) $2F_O$–$F_C$ map of belzutifan contoured at 1σ. (E–G) Structures of HIF-2α PAS-B domains in complex with belzutifan (E), PT2385 (F), or in *apo* state (G). (H) Comparison of key residue side-chain conformations in the HIF-2α PAS-B domains among *apo*, belzutifan-bound, and PT2385-bound proteins.

HIF-2α–ARNT proteins, HIF-2α inhibitors can only partially separate the two subunits, possibly due to the biochemical nature of these dimeric proteins, consistent with our previous hydrogen–deuterium exchange assay showing that inhibitors mainly destabilized HIF-2α–ARNT at the dimer interface regions rather than globally (Wu et al., 2019).

Next, we explored the inhibitory effects of belzutifan on HIF-2α activity in cellular level. HRE (5′-ACGTG-3′), a 5-base pair short motif that often locates in the promoter or enhancer regions of HIF downstream genes, can be recognized by HIF dimers to induce gene expression in response to hypoxia. We used a ccRCC 786-O cell line that was stably transfected with an HRE luciferase reporter to determine the transcriptional activity of HIF-2α. Belzutifan was found to inhibit the HIF-2α activity in a dose-dependent manner, with an $IC_{50}$ value of 17 nM (Fig. 4C), slightly lower than the $IC_{50}$ value of PT2385

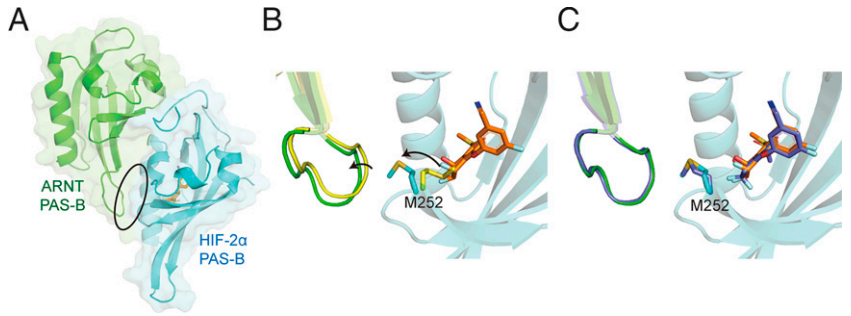


**Figure. 3** Allosteric effects of belzutifan revealed by crystal structures. (A) The overall arrangement of ARNT (green) and HIF-2α (cyan) PAS-B domains, with the location of dimer interface affected by belzutifan highlighted by an ellipse. (B) Conformational differences between belzutifan-bound and *apo* (PDB ID: 4ZP4, yellow) HIF-2α–ARNT complexes. (C) Position comparison of M252 side chain in belzutifan-bound and PT2385-bound (PDB ID: 6E3S, blue) HIF-2α–ARNT complexes.

(42 nM) measured with an identical assay previously (Wu et al., 2019).

We then determined the inhibitory effects of belzutifan on the mRNA transcription of HIF-2α target genes by a quantitative PCR assay. The overexpression of HIF-2α in the 786-O cell line due to *VHL* deficiency causes an increased expression of HIF downstream genes, thus improving the survival ability of cancer cells. Belzutifan inhibited the transcription of HIF-2α downstream genes (*CyclinD1*, *NDRG1*, *VEGFA*, and *GLUT1)* in 786-O cells in a dose-dependent manner (Fig. 4D). Besides, belzutifan could also inhibit the transcription of HIF-2α downstream genes in the HEK293 cell line, which is a noncancer cell line (Fig. 4E). It is noteworthy that the inhibitory activity of belzutifan in HEK293 cells was weaker than that in 786-O cells, which may be due to the varied responses of different cell lines to HIF-2α signal. To further reveal the key effect of M252 in regulating the interactions between HIF-2α and ARNT, we transfected the full-length HIF-2α WT or M252A mutant plasmids into Hep3B cells and measured the mRNA expression levels of HIF-2α downstream genes. As shown in Fig. 4F, the cells transfected with HIF-2α mutant M252A barely showed inhibitory effects by belzutifan, in contrast to the cells transfected with WT HIF-2α.

These structural, biochemical and functional assays together indicate that belzutifan reduces the transcriptional activity of HIF-2α by allosterically disrupting its dimerization with ARNT

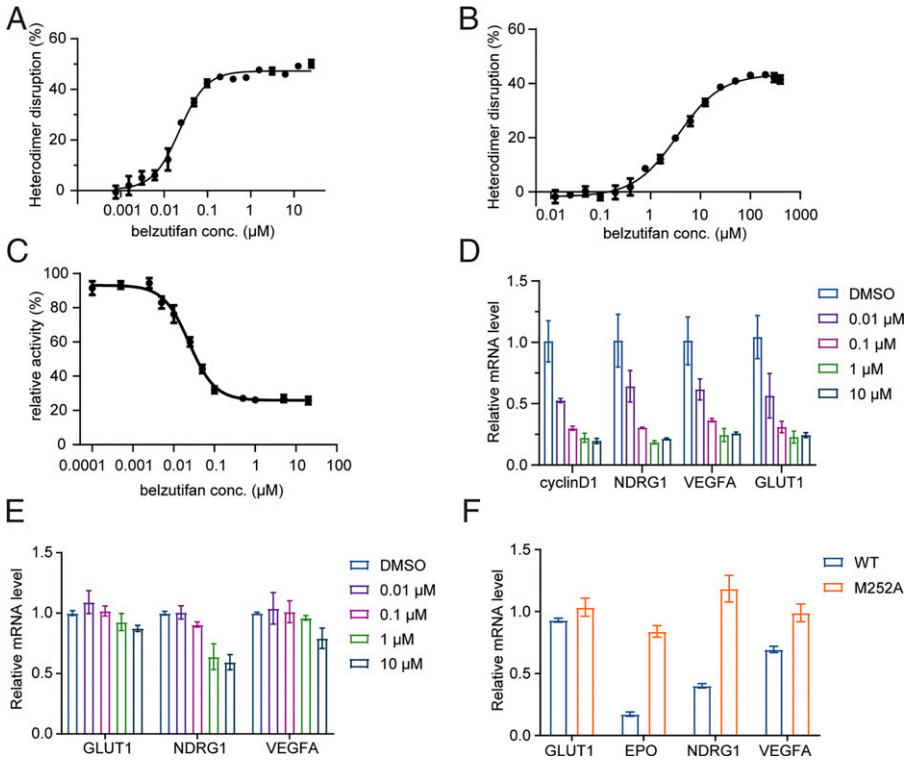


**Fig. 4.** Inhibition of HIF-2α by belzutifan. (A and B) Disruption of HIF-2α–ARNT dimers containing WT HIF-2α (A) or M252A mutant (B) by belzutifan measured using TR-FRET. Error bars, mean ± S.D. (n = 3). The $K_i$ values were derived from a four-parameter logistic equation. $K_i$ = 23 ± 1.5 nM, slope factor = 1.3 ± 0.1 (A) and $K_i$ = 3.5 ± 0.2 μM, slope factor = 1.0 ± 0.1 (B). (C) Dose-dependent inhibition of HRE luciferase reporter activity by belzutifan. Error bars, mean ± S.D. (n = 3). The $IC_{50}$ value was derived from a four-parameter logistic equation, $IC_{50}$ = 17 ± 1.6 nM, slope factor = −1.4 ± 0.1. (D and E) Expression of certain HIF-2α target genes in 786-O (D) or HEK293 (E) cells after treatment by belzutifan at various concentrations (0.01, 0.1, 1, or 10 μM). Error bars, mean ± S.D. (n = 3) (distinct replicates for cell cultures). (F) Comparison of the inhibitory effects of 10 μM belzutifan on HIF-2α target genes in Hep3B cells transfected with WT HIF-2α or M252A mutant. Error bars, mean ± S.D. (n = 3) (distinct replicates for cell cultures).

to an extent similar to PT2385 in vitro. Therefore, the efficacy improvement from PT2385 to belzutifan in clinical trials mainly come from the increased resistance to drug metabolism by the chemical modification.

## Discussion

In this work, we solved the co-crystal structure of HIF-2α–ARNT-belzutifan and revealed the inhibitory mechanism of belzutifan at molecular level. During the crystallization experiments, we found it very challenging to obtain co-crystals of HIF-2α–ARNT-belzutifan. Routine co-crystallization trials for HIF-2α–ARNT proteins and belzutifan were not successful, and even soaking of belzutifan for a long time would cause the dissolution of preformed protein crystals, which also indicates that the destabilizing effects of belzutifan on the HIF-2α–ARNT complex was fairly strong. Therefore, we had to rely on a proper soaking condition to obtain diffractable crystals, in which likely only limited drug-induced protein conformational changes were tolerated and exhibited. However, we still believe these conformational changes shown in crystal structures (especially those near the dimerization interface) reflect the possible changes in solution, as our previous hydrogen deuterium exchange mass spectrometry results correlated with the crystal structures very well (Wu et al., 2019).

Belzutifan is the first HIF-2α small-molecule inhibitor approved by Food and Drug Administration to treat the VHL disease under certain conditions. In addition, several other indications have also been investigated for the application of belzutifan. For instance, the efficacy and safety of belzutifan monotherapy in participants with advanced pheochromocytoma/paraganglioma or pancreatic neuroendocrine tumor are undergoing a phase 2 study (NCT04924075). The safety and efficacy of belzutifan in combination with pembrolizumab and lenvatinib in multiple solid tumors including hepatocellular carcinoma, colorectal cancer, pancreatic ductal adenocarcinoma, and biliary tract cancer are currently in a phase 2 clinical trial (NCT04976634). The *New England Journal of Medicine* reported a case of treating Pacak-Zhuang syndrome with belzutifan recently (Kamihara et al., 2021). The genomic testing revealed an *EPAS1* (encoding HIF2α) variant, c.1589C→A (p.A530E) in the patients, which led to the decreased HIF-2α protein degradation and enhanced hypoxia-related genes expression. Treatment with belzutifan effectively decreased plasma levels of normetanephrine and chromogranin A, improved the polycythemia, and shrank tumor rapidly. The patients experienced minimal side effects, and no grade 3 or 4 adverse events occurred during 24 months of belzutifan treatment without any interruption or dose modification (Kamihara et al., 2021).

Drug resistance is always a great challenge in the treatment of cancers. A preclinical study in ccRCC tumorgraft mice has showed that prolonged treatment with PT2399, an analog of belzutifan, caused resistance of tumor cells with two leading mutations (G323E of HIF-2α and F446L of ARNT) (Chen et al., 2016). Furthermore, HIF-2α G323E mutation was also identified in ccRCC patients treated with PT2385 (Courtney et al., 2020). Biochemical experiments and in vivo studies revealed that G323E mutation, with a much bulker side chain, could effectively prevent HIF-2α–ARNT dissociation by blocking the entry of PT2385 into the HIF-2α PAS-B pocket (Wu et al., 2019; Courtney et al., 2020). As a novel pharmacologic agent targeting HIF-2α, belzutifan exhibited a good activity against RCC in clinical trials. Although some of the patients treated with belzutifan had progressive disease, the mechanism of possible drug resistance is still unknown (Jonasch et al., 2021). Belzutifan and its analogs are a series of indonols, which have great similarities in structure (Xu et al., 2019). Our crystal structure suggests that belzutifan and PT2385 share a similar binding mode and inhibitory mechanism. Therefore, belzutifan and its upcoming analogs may also be affected by HIF-2α G323E and ARNT F446L mutations. Future research may focus on the discovery of HIF-2α inhibitors with novel chemical structures and ideally targeting different binding pockets of HIF-2α.

In addition to tumors, recent studies have revealed that HIF-2α is associated with a series of metabolic diseases. Xie et al. (2017) reported that intestinal HIF-2α activation contributes to the progression of nonalcoholic fatty liver disease through a HIF-2α–neuraminidase 3-ceramide axis. Furthermore, PT2385 could effectively improve metabolic disorders in high-fat diet–fed mice, suggesting intestinal HIF-2α may serve as a potential target for the treatment of hepatic steatosis. In addition, hepatocyte HIF-2α activation also contributes to the nonalcoholic fatty liver disease progression through upregulation of histidine-rich glycoprotein production (Morello et al., 2018). Wu et al. (2021) reported that intestinal HIF-2α deficiency could reshape the gut microbiome to enhance white adipose tissue thermogenesis through adipose G protein-coupled bile acid receptor activation, suggesting a new strategy to treat metabolic diseases by HIF-2α inhibition. These studies imply that HIF-2α inhibitors might play a pivotal role in the treatment of metabolic diseases besides their well-known antitumor activity.

#### Acknowledgments

We thank Zhifeng Li, Jing Zhu, and Xiaoju Li from State Key laboratory of Microbial Technology of Shandong University for their help and guidance in the experiments of ITC, real-time polymerase chain reaction, and X-ray diffraction. We also thank the staffs from BL19U1 beamline of National Facility for Protein Science in Shanghai (NFPS) at Shanghai Synchrotron Radiation Facility, for their assistance during data collection.

#### Authorship Contributions

*Participated in research design:* Wu, Zhuang, Ren.
*Conducted experiments:* Ren, Diao.
*Performed data analysis:* Ren, Diao.
*Wrote or contributed to writing the paper:* Wu, Zhuang.

#### References

Adams PD, Afonine PV, Bunkóczi G, Chen VB, Davis IW, Echols N, Headd JJ, Hung LW, Kapral GJ, Grosse-Kunstleve RW, et al. (2010) PHENIX: a comprehensive Python-based system for macromolecular structure solution. *Acta Crystallogr D Biol Crystallogr* **66**:213–221.

Bangoura G, Liu ZS, Qian Q, Jiang CQ, Yang GF, and Jing S (2007) Prognostic significance of HIF-2alpha/EPAS1 expression in hepatocellular carcinoma. *World J Gastroenterol* **13**:3176–3182.

Chen VB, Arendall WB 3rd, Headd JJ, Keedy DA, Immormino RM, Kapral GJ, Murray LW, Richardson JS, and Richardson DC (2010) MolProbity: all-atom structure validation for macromolecular crystallography. *Acta Crystallogr D Biol Crystallogr* **66**:12–21.

Chen W, Hill H, Christie A, Kim MS, Holloman E, Pavia-Jimenez A, Homayoun F, Ma Y, Patel N, Yell P, et al. (2016) Targeting renal cell carcinoma with a HIF-2 antagonist. *Nature* **539**:112–117.

Courtney KD, Ma Y, Diaz de Leon A, Christie A, Xie Z, Woolford L, Singla N, Joyce A, Hill H, Madhuranthakam AJ, et al. (2020) HIF-2 complex dissociation, target inhibition, and acquired resistance with PT2385, a first-in-class HIF-2 inhibitor, in patients with clear cell renal cell carcinoma. *Clin Cancer Res* **26**:793–803.

Emsley P, Lohkamp B, Scott WG, and Cowtan K (2010) Features and development of Coot. *Acta Crystallogr D Biol Crystallogr* **66**:486–501.

Esteban MA, Tran MG, Harten SK, Hill P, Castellanos MC, Chandra A, Raval R, O'brien TS, and Maxwell PH (2006) Regulation of E-cadherin expression by VHL and hypoxia-inducible factor. *Cancer Res* **66**:3567–3575.

Gordan JD, Thompson CB, and Simon MC (2007) HIF and c-Myc: sibling rivals for control of cancer cell metabolism and proliferation. *Cancer Cell* **12**:108–113.
Gu YZ, Moran SM, Hogenesch JB, Wartman L, and Bradfield CA (1998) Molecular characterization and chromosomal localization of a third alpha-class hypoxia inducible factor subunit, HIF3alpha. *Gene Expr* **7**:205–213.
Huang LE, Gu J, Schau M, and Bunn HF (1998) Regulation of hypoxia-inducible factor 1alpha is mediated by an O2-dependent degradation domain via the ubiquitin-proteasome pathway. *Proc Natl Acad Sci USA* **95**:7987–7992.
Jonasch E, Donskov F, Iliopoulos O, Rathmell WK, Narayan VK, Maughan BL, Oudard S, Else T, Maranchie JK, Welsh SJ, et al.; MK-6482-004 Investigators (2021) Belzutifan for renal cell carcinoma in von Hippel-Lindau disease. *N Engl J Med* **385**:2036–2046.
Kabsch W (2010) Integration, scaling, space-group assignment and post-refinement. *Acta Crystallogr D Biol Crystallogr* **66**:133–144.
Kamihara J, Hamilton KV, Pollard JA, Clinton CM, Madden JA, Lin J, Imamovic A, Wall CB, Wassner AJ, Weil BR, et al. (2021) Belzutifan, a potent HIF2α inhibitor, in the Pacak-Zhuang syndrome. *N Engl J Med* **385**:2059–2065.
Key J, Scheuermann TH, Anderson PC, Daggett V, and Gardner KH (2009) Principles of ligand binding within a completely buried cavity in HIF2alpha PAS-B. *J Am Chem Soc* **131**:17647–17654.
Liu YL, Yu JM, Song XR, Wang XW, Xing LG, and Gao BB (2006) Regulation of the chemokine receptor CXCR4 and metastasis by hypoxia-inducible factor in non small cell lung cancer cell lines. *Cancer Biol Ther* **5**:1320–1326.
Luan Y, Gao C, Miao Y, Li Y, Wang Z, and Qiu X (2013) Clinicopathological and prognostic significance of HIF-1α and HIF-2α expression in small cell lung cancer. *Pathol Res Pract* **209**:184–189.
McCoy AJ, Grosse-Kunstleve RW, Adams PD, Winn MD, Storoni LC, and Read RJ (2007) Phaser crystallographic software. *J Appl Cryst* **40**:658–674.
Morello E, Sutti S, Foglia B, Novo E, Cannito S, Bocca C, Rajsky M, Bruzzì S, Abate ML, Rosso C, et al. (2018) Hypoxia-inducible factor 2α drives nonalcoholic fatty liver progression by triggering hepatocyte release of histidine-rich glycoprotein. *Hepatology* **67**:2196–2214.
Rankin EB, Biju MP, Liu Q, Unger TL, Rha J, Johnson RS, Simon MC, Keith B, and Haase VH (2007) Hypoxia-inducible factor-2 (HIF-2) regulates hepatic erythropoietin in vivo. *J Clin Invest* **117**:1068–1077.
Rogers JL, Bayeh L, Scheuermann TH, Longgood J, Key J, Naidoo J, Melito L, Shokri C, Frantz DE, Bruick RK, et al. (2013) Development of inhibitors of the PAS-B domain of the HIF-2α transcription factor. *J Med Chem* **56**:1739–1747.
Sato Y, Yoshizato T, Shiraishi Y, Maekawa S, Okuno Y, Kamura T, Shimamura T, Sato-Otsubo A, Nagae G, Suzuki H, et al. (2013) Integrated molecular analysis of clear-cell renal cell carcinoma. *Nat Genet* **45**:860–867.
Scheuermann TH, Li Q, Ma HW, Key J, Zhang L, Chen R, Garcia JA, Naidoo J, Longgood J, Frantz DE, et al. (2013) Allosteric inhibition of hypoxia inducible factor-2 with small molecules. *Nat Chem Biol* **9**:271–276.
Scheuermann TH, Stroud D, Sleet CE, Bayeh L, Shokri C, Wang H, Caldwell CG, Longgood J, MacMillan JB, Bruick RK, et al. (2015) Isoform-selective and stereoselective inhibition of hypoxia inducible factor-2. *J Med Chem* **58**:5930–5941.
Scheuermann TH, Tomchick DR, Machius M, Guo Y, Bruick RK, and Gardner KH (2009) Artificial ligand binding within the HIF2alpha PAS-B domain of the HIF2 transcription factor. *Proc Natl Acad Sci USA* **106**:450–455.
Shen C and Kaelin WG Jr (2013) The VHL/HIF axis in clear cell renal carcinoma. *Semin Cancer Biol* **23**:18–25.
Tian H, McKnight SL, and Russell DW (1997) Endothelial PAS domain protein 1 (EPAS1), a transcription factor selectively expressed in endothelial cells. *Genes Dev* **11**:72–82.
Wang GL, Jiang BH, Rue EA, and Semenza GL (1995) Hypoxia-inducible factor 1 is a basic-helix-loop-helix-PAS heterodimer regulated by cellular O2 tension. *Proc Natl Acad Sci USA* **92**:5510–5514.
Wehn PM, Rizzi JP, Dixon DD, Grina JA, Schlachter ST, Wang B, Xu R, Yang H, Du X, Han G, et al. (2018) Design and activity of specific hypoxia-inducible factor-2α (HIF-2α) inhibitors for the treatment of clear cell renal cell carcinoma: discovery of clinical candidate ( S)-3-((2,2-difluoro-1-hydroxy-7-(methylsulfonyl)-2, 3-dihydro-1 H-inden-4-yl)oxy)-5-fluorobenzonitrile (PT2385). *J Med Chem* **61**:9691–9721.
Winter SC, Shah KA, Han C, Campo L, Turley H, Leek R, Corbridge RJ, Cox GJ, and Harris AL (2006) The relation between hypoxia-inducible factor (HIF)-1alpha and HIF-2alpha expression with anemia and outcome in surgically treated head and neck cancer. *Cancer* **107**:757–766.
Wu D, Potluri N, Lu J, Kim Y, and Rastinejad F (2015) Structural integration in hypoxia-inducible factors. *Nature* **524**:303–308.
Wu D and Rastinejad F (2017) Structural characterization of mammalian bHLH-PAS transcription factors. *Curr Opin Struct Biol* **43**:1–9.
Wu D, Su X, Lu J, Li S, Hood BL, Vasile S, Potluri N, Diao X, Kim Y, Khorasanizadeh S, et al. (2019) Bidirectional modulation of HIF-2 activity through chemical ligands. *Nat Chem Biol* **15**:367–376.
Wu Q, Liang X, Wang K, Lin J, Wang X, Wang P, Zhang Y, Nie Q, Liu H, Zhang Z, Liu J, Pang Y and Jiang C (2021) Intestinal hypoxia-inducible factor 2alpha regulates lactate levels to shape the gut microbiome and alter thermogenesis. *Cell Metab* **33**:1988–2003.e1987.
Xia G, Kageyama Y, Hayashi T, Kawakami S, Yoshida M, and Kihara K (2001) Regulation of vascular endothelial growth factor transcription by endothelial PAS domain protein 1 (EPAS1) and possible involvement of EPAS1 in the angiogenesis of renal cell carcinoma. *Cancer* **91**:1429–1436.
Xie C, Yagai T, Luo Y, Liang X, Chen T, Wang Q, Sun D, Zhao J, Ramakrishnan SK, Sun L, et al. (2017) Activation of intestinal hypoxia-inducible factor 2α during obesity contributes to hepatic steatosis. *Nat Med* **23**:1298–1308.
Xu R, Wang K, Rizzi JP, Huang H, Grina JA, Schlachter ST, Wang B, Wehn PM, Yang H, Dixon DD, et al. (2019) 3-[(1*S*,2*S*,3*R*)-2,3-difluoro-1-hydroxy-7-methylsulfonylindan-4-yl]oxy-5-fluorobenzonitrile (PT2977), a hypoxia-inducible factor 2α (HIF-2α) inhibitor for the treatment of clear cell renal cell carcinoma. *J Med Chem* **62**:6876–6893.
Yoshimura H, Dhar DK, Kohno H, Kubota H, Fujii T, Ueda S, Kinugasa S, Tachibana M, and Nagasue N (2004) Prognostic impact of hypoxia-inducible factors 1alpha and 2alpha in colorectal cancer patients: correlation with tumor angiogenesis and cyclooxygenase-2 expression. *Clin Cancer Res* **10**:8554–8560.
Zhang Q, Yan Q, Yang H, and Wei W (2019) Oxygen sensing and adaptability won the 2019 Nobel Prize in Physiology or medicine. *Genes Dis* **6**:328–332.
Zhang W-Z, Tang J-C, Wang S-S, Wang Z-J, Qin W-M, and He J-H (2019b) The protein complex crystallography beamline (BL19U1) at the Shanghai Synchrotron Radiation Facility. *Nucl Sci Tech* **30**:170.
Zhao J, Du F, Shen G, Zheng F, and Xu B (2015) The role of hypoxia-inducible factor-2 in digestive system cancers. *Cell Death Dis* **6**:e1600.

**Address correspondence to:** Dalei Wu, State Key Laboratory of Microbial Technology, Shandong University, 72 Binhai Road, Qingdao 266237, China. E-mail: dlwu@sdu.edu.cn; or Jingjing Zhuang, State Key Laboratory of Microbial Technology, Shandong University, 72 Binhai Road, Qingdao 266237, China. E-mail: zhuangjj929@sdu.edu.cn